sciendo

JAISCR, 2024, Vol. 14, No. 1, pp. 77 – 95
10.2478/jaiscr-2024-0005

A FEW-SHOT LEARNING APPROACH FOR COVID-19 DIAGNOSIS USING QUASI-CONFIGURED TOPOLOGICAL SPACES

Hui Liu[1,2], Chunjie Wang[1], Xin Jiang[3], Mohammad Khishe[4,*]

[1]*School of Mathematics and Statistics, Changchun University of Technology, Changchun 130012, Jilin, China*

[2]*School of Economics and Management, Changchun University of Technology, Changchun 130012, Jilin, China*

[3]*Department of Biochemistry, College of Basic Medical Sciences, Jilin University, Changchun 130021, Jilin, China*

[4]*Department of Electrical Engineering, Imam Khomeini Marine Science University, Nowshahr, Iran*

[*]*E-mail: m_khishe@alumni.iust.ac.ir*

Submitted: 14th April 2023; Accepted: 13th December 2023

Abstract

Accurate and efficient COVID-19 diagnosis is crucial in clinical settings. However, the limited availability of labeled data poses a challenge for traditional machine learning algorithms. To address this issue, we propose Turning Point (TP), a few-shot learning (FSL) approach that leverages high-level turning point mappings to build sophisticated representations across previously labeled data. Unlike existing FSL models, TP learns using quasi-configured topological spaces and efficiently combines the outputs of diverse TP learners. We evaluated TPFSL using three COVID-19 datasets and compared it with seven different benchmarks. Results show that TPFSL outperformed the top-performing benchmark models in both one-shot and five-shot tasks, with an average improvement of 4.50% and 4.43%, respectively. Additionally, TPFSL significantly outperformed the ProtoNet benchmark by 12.966% and 11.033% in one-shot and five-shot classification problems across all datasets. Ablation experiments were also conducted to analyze the impact of variables such as TP density, network topology, distance measure, and TP placement. Overall, TPFSL has the potential to improve the accuracy and speed of diagnoses for COVID-19 in clinical settings and can be a valuable tool for medical professionals.

Keywords: COVID-19, medical diagnosis, Quasi-Configured Topological Spaces, few-shot learning

1 Introduction

The COVID-19 pandemic has caused a significant global health crisis, with millions of confirmed cases and fatalities worldwide [1, 2]. Early diagnosis and accurate classification of COVID-19 patients are crucial for effective treatment and prevention of its spread [3]. However, the lack of large-

scale COVID-19 datasets poses a significant challenge to developing accurate classification models [4]. In recent years, deep learning (DL) models have shown promising results in various medical image analysis tasks [5–7], including COVID-19 [8], electroencephalogram (EEG) classification[9], situation-aware service [10], chronic care [11], surgical instrument localization algorithm [12], and lipid-poor adrenal adenoma [13].

Achieving human-level performance on COVID-19 diagnosis tasks with a limited number of annotated examples remains a significant challenge for deep learning (DL) [14]. With little training data, models are often too simplistic or overfit, leading to poor generalization [15, 16]. Humans, in contrast, can acquire novel skills quickly by using their experience and knowledge [17]. The ability to adapt is a sign of intelligence in individuals [18].

To address this challenge, few-shot learning (FSL) algorithms have been designed to generalize to new tasks, given only a few labeled training examples [19]. Recent advances in meta-learning (MeL) have explicitly optimized the model's ability to generalize by acquiring prior knowledge over previous tasks [20]. Nonetheless, current meta-learning techniques perform similarly to simple existing approaches according to recent research, raising concerns about the essential elements for quick adaption and generalization [21].

We propose a solution to this problem by emphasizing the importance of structured human cognition, specifically reusable TPs [22]. Humans can recognize new classes of objects by focusing on specific TPs, such as height or number of doors, and combining them to identify new species. This structured form of cognition enables humans to provide reasoning behind their decisions [23]. The lack of structure in current meta-learners limits their generalization ability [24]. Instead, we use a meta-learning technique that we call TP to find generalizable descriptions across TP aspects that humans can understand.

Through the use of threshold embedding functions, or TP learners, specified by DL models, TP learns a distinct metric space for each dimension. In order to capture class divisions in the metric space of the fundamental threshold, TP models are constructed along each high-level dimension. To produce final predictions, TP combines data from various TP learners and threshold prototypes. Our method's excellent generalizability is a result of three crucial factors: quasi-configured symbol learning, threshold-based metric spaces, and model ensembling. We can either define TPs from external knowledge bases or uncover the high-level set of TPs that will drive our algorithm entirely unsupervised. In the FSL context, where observations are based on only a small number of labeled samples, causing it to be hard to verify the model, TP's estimations are interpretable, giving it an advantage. As a result, TP is the first interpretable, domain-neutral meta-learning method.

The main contribution of the paper can be stated as follows:

- **Innovative Approach with Few-Shot Learning (FSL)**: In contrast to conventional machine learning techniques, this work presents a Turning Point (TP), a new FSL method. This method was developed in response to the difficulties associated with COVID-19 diagnosis caused by the scarcity of labeled data.
- **Utilization of Quasi-Configured Topological Spaces:** One distinctive feature of the TP approach is the utilization of quasi-configured topological spaces for education. Its revolutionary approach to constructing complex representations sets it apart from other FSL models and advances the discipline.
- **Combining Outputs of TP Learners:** The methodology for merging the outputs of different TP learners is a significant contribution that improves the learning process's efficiency and efficacy.
- **Empirical Validation with COVID-19 Datasets**: The research does more than offer a theoretical model; it also uses three COVID-19 datasets to verify the model's accuracy. This empirical testing is essential for proving the TP methodology's viability and usefulness in actual settings.
- **Benchmark Comparisons:** The comparison of TPFSL's performance to that of seven distinct benchmarks is a notable addition, as is the showing of its superior performance on one-shot and five-shot jobs. The results of this comparison

show that the TP method is superior to the alternatives.

- **Detailed Ablation Study:** The impact of factors such as TP density, network topology, distance measure, and TP location can be better understood by conducting in-depth ablation studies. This research is helpful for future studies and applications because it sheds light on the variables that affect the efficiency of the TP approach.
- **Potential for Clinical Application**: Finally, the article underlines the potential of TPFSL in enhancing the accuracy and timeliness of COVID-19 diagnoses in clinical settings. This real-world application is a significant advance since it fills a pressing need in the healthcare system during the pandemic.

The paper's structure is as follows: Part 2 presents related studies, Section 3 details the proposed methodology, Section 4 addresses experiments, and Section 5 concludes the paper.

2 Related works

The development of effective and accurate diagnostic methods for COVID-19 is of utmost importance to mitigate the spread of the disease [25, 26]. In recent years, few-shot learning has emerged as a promising approach for developing diagnostic models with limited labeled data [7]. In this section, we review some of the existing works related to few-shot learning in the context of COVID-19 diagnosis [27].

One of the earliest works in this area was a study by Wang et al. [28], which proposed a few-shot learning approach based on a Siamese network architecture to classify chest X-ray images as COVID-19 positive or negative. The authors demonstrated that their model achieved high accuracy even with a small number of labeled samples and outperformed several state-of-the-art methods.

Li et al. [29] utilized a few-shot learning approach to develop a diagnostic model for COVID-19 based on CT scans. The authors proposed a novel framework that combined a contrastive learning objective with a prototype-based classifier and showed that their model achieved competitive performance on a benchmark dataset.

In a different approach, Chen et al. [30] proposed a few-shot learning framework that incorporated domain adaptation techniques to improve the generalization of COVID-19 diagnosis models across different hospitals. The authors used a meta-learning approach to adapt their model to different domains and showed that their method outperformed several baselines.

Ge et al. [31] proposed a novel few-shot learning framework that incorporates a transformer-based meta-learner to diagnose COVID-19 from CT images. The authors demonstrated the effectiveness of their approach on a benchmark dataset.

Jiang et al. [32] developed a few-shot learning-based COVID-19 diagnosis model that combines a feature extractor with a Siamese network. The authors showed that their method outperforms several existing methods on a benchmark dataset.

Abdrakhmanov et al. [33] proposed a few-shot learning approach based on a convolutional neural network for COVID-19 diagnosis using chest X-ray images. The authors demonstrated that their method achieved high accuracy even with a small number of labeled samples.

Abdel-Basset et al. [34] developed a deep learning model for semi-supervised few-shot segmentation of COVID-19-positive cases that leverages a feature extraction network and a novel similarity measure. The authors showed that their approach outperforms several existing methods on a benchmark dataset.

Singh et al. [35] proposed a few-shot learning framework for COVID-19 diagnosis that leverages an attention-based feature embedding network and a prototype-based classifier. The authors demonstrated the effectiveness of their approach on a benchmark dataset.

Wang et al. [36] proposed a few-shot learning approach for COVID-19 diagnosis that leverages a self-attention network to extract features from chest X-ray images. The authors demonstrated the effectiveness of their approach on a benchmark dataset.

Shorfuzzaman et al. [37] developed a Siamese framework with contrastive loss for few-shot learning of COVID-19 patients. The authors showed that their approach outperforms several existing methods on a benchmark dataset.

Finally, a recent study by Abdrakhmanov et al. [38] proposed a few-shot learning approach based on a residual neural network architecture for COVID-19 diagnosis using chest X-ray images. The authors demonstrated that their method achieved high accuracy even with a limited number of labeled samples and outperformed several existing methods on a benchmark dataset.

In summary, the above studies demonstrate the potential of few-shot learning approaches for developing accurate and effective diagnostic models for COVID-19, even with limited labeled data. These methods may have important implications for improving the diagnosis and management of the disease, particularly in resource-constrained settings.

Nonetheless, these studies highlight the potential of MeL and FSL in medical diagnosis, particularly for conditions such as COVID-19 diagnosis. The proposed Turning point FSL approach presents a novel method that not only enhances interpretability but also achieves significant relative improvement on challenging FSL tasks. These approaches have promising implications for clinical use, potentially enhancing the accuracy and efficiency of diagnosis for these medical conditions.

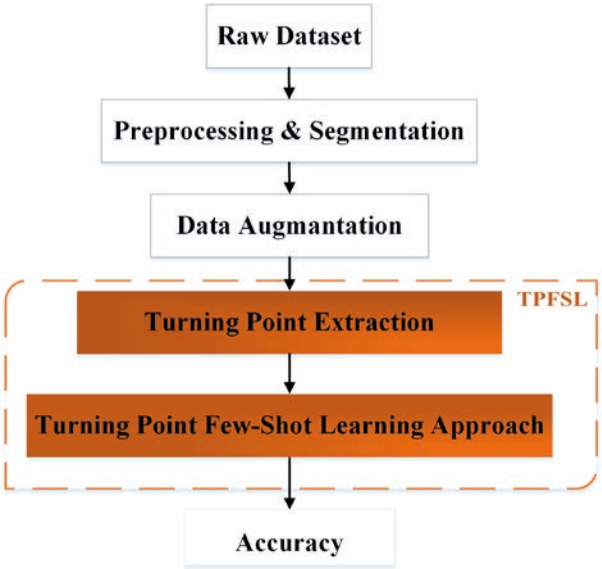

Figure 1. The block diagram of our proposed classification system.

3 Proposed methodology

The typical procedure for diagnosing COVID-19 involves two primary stages: TP extraction and classification. While DNNs are often used to classify COVID-19 diagnosis, the scarcity of available samples can pose a significant challenge. To address this issue, we have devised the TPFSL model to enhance the precision of classification. Our classification system comprises three key components: preprocessing, TP extraction, and classification. To better understand these components, please refer to the block diagram depicted in Figure 1.

3.1 Raw datasets

Two CT Scan datasets utilized in this investigation are COVCT [39] and SARSCoV2 [40], the specifics of which are covered in the following subsections.

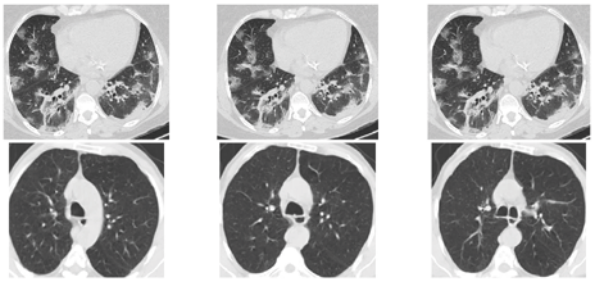

Figure 2. A sample of a CT scan from the SARSCoV2 dataset.

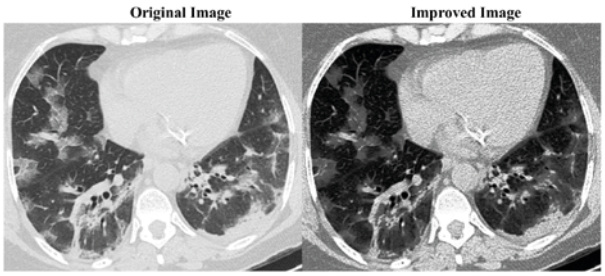

Figure 3. Two images with contrasting sizes and proportions.

3.1.1 SARSCoV2 CT-Scan dataset

In São Paulo hospitals, SARSCoV2 was discovered [40]. The dataset includes 2482 images from 120 people, 1252 CT scans of those who have SARSCoV2, and 1230 among those who do not have the virus but suffer from a range of respiratory conditions. Typical, normal, and infected cases are shown in Figure 2. Whereas the second raw contains typical (uninfected) cases, the first raw has some infected cases. It should be emphasized that, as depicted in Figure 3, the SARSCoV2 lacks ex-

ceptional homogeneity with respect to contrast and picture sizes.

3.1.2 COVCT dataset

CT scans of COVID-19-infected individuals can be found in the COVCT collection [39]. 349 images of 216 patients are included in this collection. Photos of non-COVID and healthy people were sourced from two additional datasets: LUNA and MedPix [39]. This dataset segment has 463 images of 55 people in good health. The second dataset, like the first, lacks a defined image contrast and dimension adjustment. It is a fact that the utmost care must be taken to ensure that the utmost care is given. Both the original version and the enhanced version are shown in Figure 4. The details of the utilized datasets are listed in Table 1.

3.1.3 SIRM dataset

The Italian Society of Medical and Interventional Radiology (SIRM) COVID-19 dataset is a collection of chest CT scans acquired from COVID-19-positive patients in Italy [41]. The dataset was created with the aim of providing a tool for researchers to study the radiological aspects of COVID-19 and to develop AI-based tools for the automatic detection and classification of COVID-19 cases. The SIRM COVID-19 Database contains over 4000 CT scans from more than 1200 patients, and it includes both non-contrast-enhanced and contrast-enhanced scans. The dataset is publicly available for research purposes, and it has been used in numerous studies investigating the radiological features of COVID-19 and developing AI-based tools for the automatic detection of COVID-19 cases from CT scans. The SIRM COVID-19 database is considered one of the most comprehensive and valuable resources for researchers studying COVID-19 radiology.

Considering the lack of valid data, the following image augmentation technique is used to increase the number of CT scans [42]. Some common types of image augmentation that are applied to COVID-19 CT scans include [43]:

Rotation: This involves rotating the image by a certain angle (e.g., 90 degrees) to increase the number of training examples and help the model generalize better.

Scaling: Scaling the image up or down can be helpful to increase the variability in the dataset and help the model learn to recognize COVID-19 in CT scans at different scales.

Flipping: The dataset's variability can be increased by flipping the photo horizontally or vertically, and the machine can learn to recognize COVID-19 from various angles.

Translation: Translation involves moving the image horizontally or vertically by a certain distance, which can increase the dataset's variability and help the model learn to recognize COVID-19 from different positions.

Gaussian noise: Adding random Gaussian noise to the image can help the model learn to recognize COVID-19 from noisy scans or scans with lower image quality.

Contrast adjustment: The model can learn to distinguish COVID-19 in scans with various contrast levels by adjusting the image's contrast.

Shearing: Shearing the image involves skewing the image along a particular axis, which can increase the dataset's variability and help the model learn to recognize COVID-19 from different angles.

It should be noted that LUNG CAD is utilized to segment the central part of the lung from the background. Typical results for data segmentation and augmentation are illustrated in Figures 5 and 6.

3.2 Turning point technique

Section 2 of the paper highlighted the challenge of accurately classifying COVID-19 diagnosis with DNNs when working with small datasets. To address this limitation, we propose using the TPFSL technique, which consists of two phases: TP point localization and classification. We have developed an algorithm (Algorithm 1) that provides a detailed outline of our TP point method. We will provide further elaboration on this approach.

Table 1. The details of the datasets

Dataset	No.	**COVCT** [39]	**SARSCoV2** [40]	**SIRM** [41]
COVID-19	Individuals	216	60	600
	CT scans	349	1252	2000
Healthy	Individuals	55	60	600
	CT scans	463	1230	2000

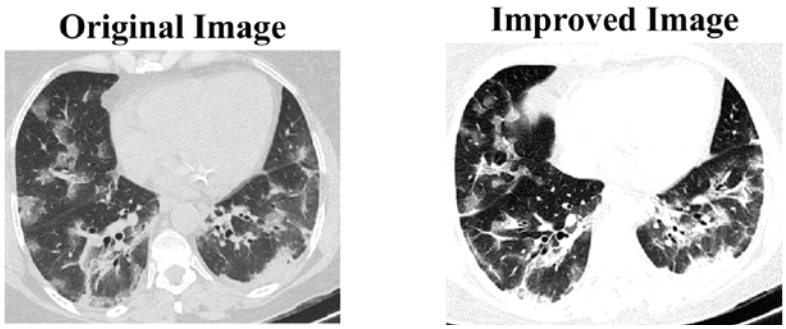

Figure 4. The original and improved CT scans.

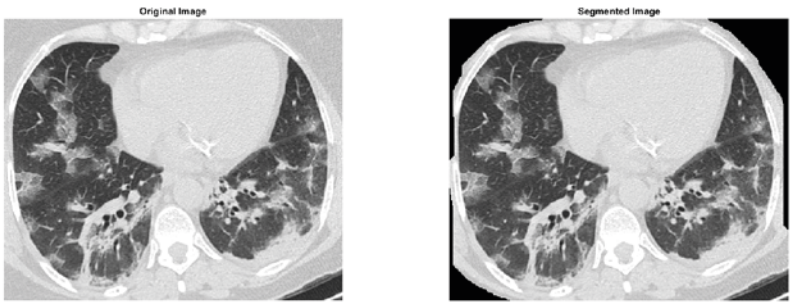

Figure 5. CT scan's segmentation

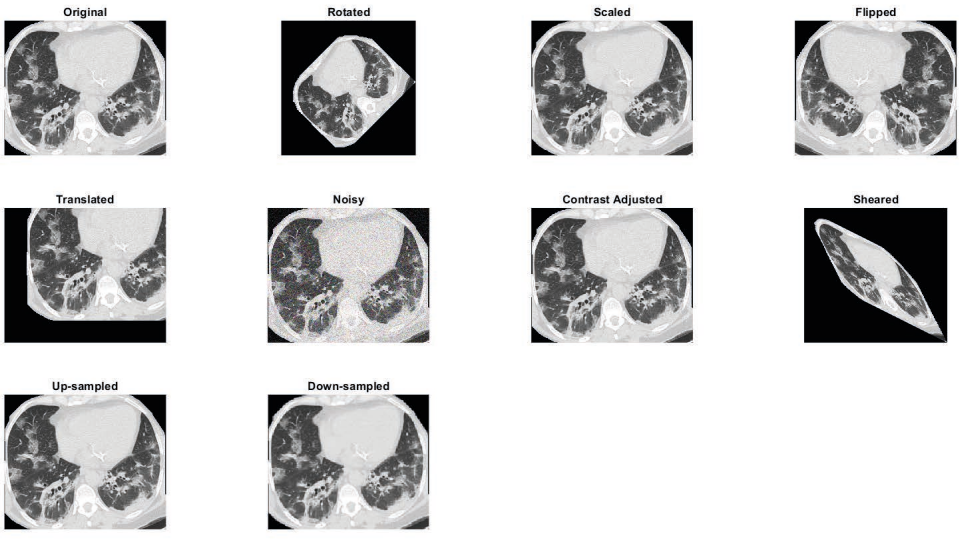

Figure 6. CT scan's augmentation.

Algorithm 1: TP Extraction Method with TPFSL for COVID-19 diagnosis

Input: CT scans
Output: TP points
for λ = 1,2, ..., TOT **do**
Define two contrast parameters to determine the threshold values based on power (in dB) at all time points.
Identify TP points by locating the points where the power changes beyond the threshold.
Extract the location of each TP point.
Represent each TP point as a vector of its coordinates.
Cluster the TP points based on their similarity to group them into different categories.
For each cluster, calculate the center of the cluster as the TP point for that category.
Classify COVID-19 CT scans by computing the distance between each signal's TP point and the center of each cluster.
Assign each signal to the category with the closest center.
end for
return the TP points $(t_n; p_n)$ and their corresponding categories

To summarize, our proposed technique for COVID-19 diagnosis involves using TP points extracted from their CT scans. These TP points are obtained by identifying power changes above a certain threshold and clustering them based on their similarity. In order to categorize the signals, we measure the separation among each TP and the center of each cluster. The proposed method for TP extraction involves identifying time points and thresholds, allowing us to locate power changes at specific points. TP locations are then saved as $(t_n; p_n)$ coordinates where t_n and p_n refer to the time and corresponding point when power is above the threshold. Our approach offers a comprehensive means of gathering vital data from COVID-19 diagnosis CT scans. Clustering TP points can help identify distinctive features and patterns that differentiate these diseases, ultimately improving their accuracy of classification.

3.3 Few-shot learning

The TPFSL methodology makes use of TP learners to create unique metric spaces for each TP dimension based on a small set of labeled real-world data. By utilizing TP prototypes as indicators of class-level distinctions in each higher-level dimension's measurement space and TP merging functions as learners, TPFSL can identify subtle variations. By incorporating various precise TP learners, the TPFSL model enhances the base learner's generalization ability.

During its operation, TPFSL utilizes three data sets: labeled training data (D_L), unlabeled query data (D_Q), and a support set (δ). Unlike the query and training sets, the support set comprises labeled datasets that exist in the same label space. A TP data point is represented as a tuple (t, p), where t denotes the label and p denotes the data point. The TPFSL approach aims to label the query set by utilizing the labeled training data and support set.

Prototypical FSL is a machine learning classification technique that is widely used and aims to generalize new tasks effectively [28]. During training, this approach uses mini-samples referred to as episodes, where a few classes are chosen from the training data for each episode, and data points are labeled accordingly. A query set, which is used to calculate prediction errors, and a support set, which consists of labeled data points, are created from the collected information [44].

During each episode, the TPFSL model aims to minimize the loss in the query group while keeping the sample group constant. This approach is beneficial for improving the model's generalization ability during the testing phase when data availability is limited. The training sets used in this process are known as "balanced episodes," which represents the number of support points per class (also known as "shot"), and represents the number of classes per episode (known as "way") [45].

In the TPFSL approach, non-linearly parameterized TP merging functions, also referred to as TP learners, are incorporated through a DNN in a non-linear fashion. Each TP learner produces TP prototypes for each class, which are computed by averaging the perceived merging of the support set's data points. This averaging enables the model to acquire a superior representation of each class, thereby enhancing its capacity to generalize.

$$CP_{\beta}^{\alpha} = \frac{1}{\Gamma_{\beta(t_n;p_n)} \in \Gamma_{\beta}} EF_{\xi}^{\alpha}(t_n \circ \mu^{\alpha}) \qquad (1)$$

In this context, the symbol represents the Hadamard product, while the symbol denotes the TP number. Consequently, a set of N TP prototypes represents each class denoted by β, denoted as $CP_{\beta\ \alpha=1}^{\alpha N} = 1$. Additionally, the set of "N" TPs extracted using the proposed TP extraction method is denoted by $\mu_{\alpha_{\alpha=1}}^{N} = \Gamma$. The TPs serve as prior knowledge to assist the model in creating a more precise representation of each class. Figure 7 depicts how TPFSL learns TP merging across each dimension and assigns TP importance grades to each dimension by comparing independent TP learners and TP prototypes.

TPFSL employs an interpretability method that assigns importance grades to both local and global TPs for each class. Local importance grades are assigned based on the TP merging of a query data point with TP prototypes, giving higher grades to TPs that contribute more to the query point's classification.

This approach enables TPFSL to provide direct reasoning for each prediction by utilizing the local grades. For global explanations, the model calculates the average distance between the TP prototype and the TP merging of the query points of interest, producing an inverse average distance that represents the global TP significance grade. By ranking the TPs based on this grade, it is possible to identify essential TPs across a set of examples and gain insights.

Moreover, TPFSL can rank points based on their similarity to a fixed TP, making it possible to identify locally similar examples both within and outside of the same class. This feature is handy for identifying examples that are representative of the TP prototype or those that are dissimilar from it.

4 Experimentation and discussion

To conduct our analysis, we applied the TPFSL method to two distinct datasets, each of which consists of 25 parts or TPs. However, some of the images in the datasets were missing certain TPs. In such instances, we substituted the missing TP with a prototypical one. With the help of part coordinates, we generated a TP mask that covered the surrounding bounding box with a fixed length.

4.1 Experimental setup

To evaluate the effectiveness of TPFSL, we compared its performance against seven different benchmarks, including MCFSL [30], SUFSL [46], MAMIFSL [47], DCRFSL [35], IFSL [48], MKFSL [49], and ProtoNet [50].

In this study, we used the commonly employed 2-way classification task to evaluate the models. The support set comprised k examples for each class, where k is the number of shots, while the query set consisted of 5 unlabeled samples belonging to the support set's classes. The top model was selected using validation accuracy, and performance was evaluated using a test set of novel classifications. Specifically, we used the evaluation technique described in [51], which separated the data into 50% basic, 25% validation, and 25% test sets while maintaining the same split each time.

For our implementation, we adopted the Conv-4 architecture, which consists of four convolutional layers and an input size of 84 × 84, following the recommendation of [50]. For all datasets, we employed Adam as our optimizer of choice, setting the initial learning rate to 10-3 and the weight decay to 0. A total of 40,000 episodes were used in training for the 5-shot tasks, while 60,000 episodes were used in training for the 1-shot tasks, as is commonly done [51].

To speed up the training process of the TPFSL algorithm, we utilized shared network parameters among TP learners. Specifically, the entire image is first forwarded into the convolutional network, obtaining a feature merging, then obtaining the j-th TP merging as. The option to apply the mask at the beginning or end of the process has little impact on performance, but the latter approach does speed up training time. If certain parts of an image are not annotated, we replace the missing TP with a prototypical TP corresponding to the entire image. Our network was trained for 1,000 episodes. To evaluate the performance of IFSL, RelationNet, MCFSL, SUFSL, and ProtoNet, we used the implementations provided in [51]. For MKFSL and DCRFSL, we used the implementations described

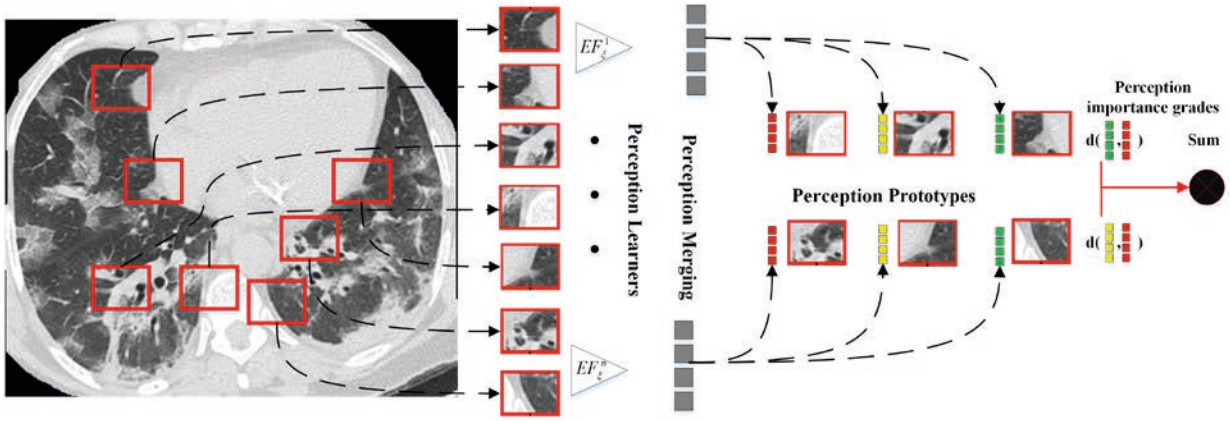

Figure 7. Illustration of how the TPFSL model learns to merge TPs along each dimension and assigns importance grades to each dimension by comparing independent TP learners with TP prototypes.

in their respective papers. We randomly sampled 600 episodes during fine-tuning or meta-testing and reported the mean accuracy on the datasets.

4.2 Performance analysis

Table 2 presents the results of our performance comparison on the mentioned datasets, where TPs serve as prior domain knowledge. TPFSL outperforms all benchmark models significantly across all datasets. In the one-shot and five-shot tasks, TPFSL achieves an average improvement of 4.50% and 4.43%, respectively, over the top-performing benchmark models. Significantly, TPFSL outperforms ProtoNet's benchmark results by 12.966% and 11.033% in the one-shot and five-shot tasks, respectively, for all datasets.

To confirm that the performance improvements of TPFSL are mainly due to the TP learners and not additional weights, we tested the impact of a deeper Conv-6 backbone on TPFSL's performance. We found that TPFSL maintains its significant performance gains even with a deeper backbone. Moreover, we compared TPFSL to an ensemble of ProtoNets and found that TPFSL outperforms the ProtoNet ensemble, even with shared weights among TPs. Additionally, we evaluated TPFSL's performance with shared weights across all TPs and observed no significant decrease in efficiency. These findings highlight the effectiveness and efficiency of TPFSL's approach. The results are summarized in Table 3.

4.3 The impact of TP quantity

Figure 8 analyses how changing the TP count affected TPFSL's effectiveness on the tested datasets. The analysis starts with ProtoNet's results, which use a single TP covering all input dimensions. Subsequently, the number of TPs gradually increased, and TPFSL was trained and evaluated accordingly. The results indicate that increasing the number of TPs enhances TPFSL's performance on all datasets.

ProtoNet's effectiveness on COVCT is enhanced by 11% and 6% in the 1-shot and 5-shot tasks, respectively, when a single TP matching to a 10 dB threshold of the entire image TP is included. TPFSL, on the other hand, outperforms all benchmark networks in SARSCOV2 with only 8 TPs, showing an 8 percentage point and 18 percentage point improvement over ProtoNet, respectively, on the 1-shot and 5-shot tasks. Also, we increased the number of TPs to 50, which included many duplicate associations, to test TPFSL's resilience to a large set of redundant TPs. As illustrated in Figure 8, even with 50 TPs, TPFSL only marginally improves performance compared to using 25 TPs. Thus, TPFSL outperforms other methods even with few TPs, inadequate annotations, and a large number of redundant and overlapping TPs.

4.4 An experiment to evaluate the distance function through ablation study

FSL heavily relies on distance metrics to gauge the resemblance between samples and to compare a new sample with a restricted set of available ex-

Table 2. The results for the one-shot and five-shot tasks on the SARSCOV2, COVCT, and SIRM datasets.

Dataset	Model	One-shot (%)	**Five-shot (%)**
SARSCOV2	ProtoNet [50]	65.60 ± 0.98	83.60 ± 0.68
	IFSL [48]	69.84 ± 1.01	84.09 ± 0.68
	MAMIFSL [47]	69.99 ± 0.99	84.44 ± 0.67
	MKFSL [49]	79.15 ± 0.99	89.23 ± 0.68
	DCRFSL [35]	79.17 ± 0.98	89.76 ± 0.68
	MCFSL [30]	79.76 ± 0.99	89.05 ± 0.67
	SUFSL [46]	76.60 ± 0.98	87.50 ± 0.68
	TPFSL (Ours)	**80.04 ± 0.98**	**92.80 ± 0.36**
COVCT	ProtoNet [50]	58.20 ± 1.08	77.20 ± 0.87
	IFSL [48]	67.88 ± 1.07	84.28 ± 0.87
	MAMIFSL [47]	68.33 ± 1.09	84.81 ± 0.87
	MKFSL [49]	68.15 ± 1.08	84.12 ± 0.87
	DCRFSL [35]	68.78 ± 1.08	84.83 ± 0.87
	MCFSL [30]	67.69 ± 1.07	83.68 ± 0.87
	SUFSL [46]	64.28 ± 1.07	82.49 ± 0.87
	TPFSL (Ours)	**69.33 ± 1.03**	**86.26 ± 0.83**
SIRM	ProtoNet [50]	59.60 ± 1.01	76.24 ± 0.76
	IFSL [48]	64.94 ± 1.00	81.02 ± 0.76
	MAMIFSL [47]	64.77 ± 1.00	80.12 ± 0.76
	MKFSL [49]	65.07 ± 1.00	81.26 ± 0.76
	DCRFSL [35]	64.98 ± 1.00	80.46 ± 0.76
	MCFSL [30]	64.78 ± 1.00	80.87 ± 0.76
	SUFSL [46]	67.07 ± 1.00	87.14 ± 0.76
	TPFSL (Ours)	**72.63 ± 1.00**	**90.27 ± 0.72**

Table 3. A comparison between the performance of the ensemble of prototypical networks and TPFSL models, where the weights are shared across TPs.

Method	COVCT		SARSCOV2		SIRM	
	1-shot	5-shot	1-shot	5-shot	1-shot	5-shot
Ensemble ProtoNet	65.1±0.9	83.4±0.6	68.3±0.9	84.7±0.6	63.5±0.8	80.4±0.4
Shared weight PML	69.3±1.0	86.2±0.6	79.3±1.1	92.1±0.6	70.9±0.9	89.7±0.4
PML	69.3±1.0	86.2±0.6	80.0±1.0	92.8±0.6	72.6±0.8	90.3±0.4

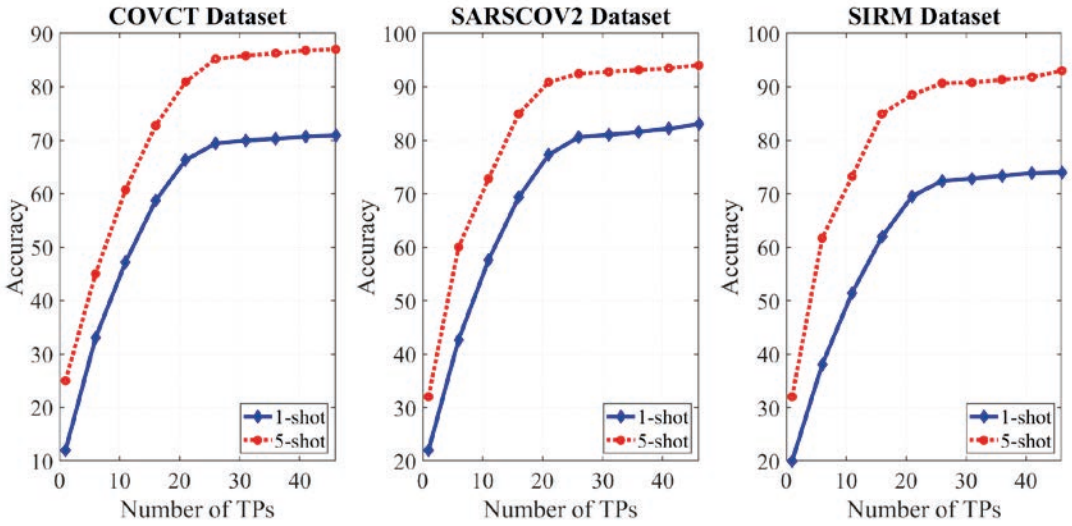

Figure 8. The impact of TP quantity

amples. To gauge the distance function's contribution to the model's general efficiency, we conducted an ablation study. The study involved systematically replacing the distance function and assessing its impact on the model's accuracy. Based on the results of the ablation study, we determined the significance of the distance function and its effect on the model's performance. FSL employs a range of distance metrics, including Euclidean distance, Manhattan distance, Mahalanobis distance, and cosine distance:

– **Euclidean distance**: Euclidean distance is a prevalent distance metric utilized in FSL. This metric estimates the direct distance between two points in a multi-dimensional space. The Euclidean distance between two vectors, **u** and **v**, is computed as the square root of the sum of the squared differences between corresponding elements in both vectors. The formula for calculating the Euclidean distance is as follows:

$$d_E(u,v) = \sqrt{\sum_i (u_i - v_i)^2} \tag{2}$$

Where u_i and v_i are the i-th elements of the vectors **u** and **v**, respectively, and i is in the range of length (**u**).

– **Manhattan distance**: The Manhattan distance, which is also referred to as the city block distance, is a distance metric used in FSL. This metric estimates the distance between two points by summing the absolute differences between their respective coordinates. In order to calculate the Manhattan distance between two vectors, **u** and **v**, the absolute difference between the corresponding elements of both vectors is first computed. The resulting differences are then summed up to get the Manhattan distance between the two vectors. The formula for computing the Manhattan distance is given below:

$$d_M(u,v) = \sum_i u_i - v_i \tag{3}$$

– **Cosine distance**: The cosine distance, which is also referred to as cosine similarity, is another distance metric used in FSL. This metric measures the similarity between two vectors based on the cosine of the angle between them. In order to calculate the cosine distance between two vectors, the dot product of the two vectors is first computed. The result is then divided by the product of the magnitudes of both vectors. The formula for computing the cosine distance is given below [52]:

$$d_c(u,v) = 1 - \frac{u \cdot v}{\|u\| \, \|v\|} = \frac{\sum_i u_i v_i}{\sqrt{\sum_i u_i^2} \sqrt{\sum_i v_i^2}} \tag{4}$$

where is the dot product of u and v, and $||\mathbf{u}||$ and $||\mathbf{v}||$ are the Euclidean norms of **u** and **v**, respectively.

– **Mahalanobis distance**: The Mahalanobis distance is yet another distance metric utilized in

FSL. This metric calculates the distance between two vectors by considering the covariance matrix of the distribution. In order to calculate the Mahalanobis distance between two vectors, **u** and **v**, the squared differences between their corresponding elements are first computed. The resulting differences are then normalized by the covariance matrix C of the distribution. Finally, the square root of the sum of the normalized squared differences is computed to obtain the Mahalanobis distance between the two vectors. The formula for computing the Mahalanobis distance is given below [53]:

$$d_{MA}(u,v) = \sqrt{(u-v)^T \cdot inv(C) \cdot (u-v)} \quad (5)$$

Where C is the covariance matrix of the data and $inv(C)$ is its inverse.

We examined the impact of different distance metrics on the classification performance of TPFSL, and the outcomes are outlined in Table 4. The results indicated that the Euclidean distance exhibited superior accuracy compared to other metrics across all experiments.

4.5 An experiment to evaluate the backbone network through ablation study

Table 5. The performance results obtained using the Conv-6 backbone on the COVCT dataset.

Method	COVCT	
	1-shot	5-shot
SUFSL	67.1±1.0	83.1±0.7
MCFSL	67.6±1.0	79.3±0.7
IFSL	67.4±1.2	79.9±0.8
MAMIFSL	65.5±1.0	81.5±0.7
MKFSL	66.6±1.3	84.2±0.9
DCRFSL	67.9±1.0	82.3±0.8
ProtoNet	67.7±1.1	83.1±0.7
TPFSL/1 TP	70.0±1.0	84.9±0.7
TPFSL	**73.3±1.0**	**88.8±0.6**

An ablation study was performed on the backbone network to compare the performance of TPFSL with benchmark methods. For the COVCT dataset, we utilized a deeper Conv-6 backbone instead of the Conv-4 backbone and employed part-based markers to identify TPs. The results of the study are presented in Table 5, where we report the average and variance for 600 randomly chosen episodes. The outcomes indicate that TPFSL achieved superior performance compared to all other models, even with the use of a deeper backbone. Furthermore, incorporating the most commonly used TP, which corresponds to a 20 dB threshold, along with the whole image TP, resulted in a 5.6% and 5.5% improvement in ProtoNet's accuracy for the one-shot and five-shot tasks, respectively.

4.6 The evaluation of the TP's locations

To assess the efficacy of TPFSL in utilizing visually extracted TPs on the datasets, we utilized the auto-encoding methodology for feature discovery proposed in [54]. We employed the authors' provided implementation and default parameters, selecting 25 features. The encoding module generated coordinates for the estimated features, which were used to generate a TP mask by creating a bounding box around the detected features. The auto-encoder was trained using the same parameters as [54]. We compared the results of one-shot and five-shot classification on the three datasets using randomly chosen masks as TPs and human-defined TPs. The outcomes, including the average accuracy (AVE) and standard deviation (STD) calculated from 600 randomly chosen episodes, are reported in Table 6. Additionally, Figure 9 depicts examples of extracted features from six different images across all datasets.

The presented table displays the results of an experiment that compared the effectiveness of three distinct methods, namely SARSCOV2, COVCT, and SIRM, in distinguishing between randomly chosen masks and masks defined by humans. The table showcases the accuracy (AVE ± STD) of each method in recognizing the masks using two protocols: one-shot and five-shot. The outcomes indicate that human-defined masks performed better than random masks in all cases, as expected. Specifically, the accuracy of human-defined masks was superior to that of random masks for all three methods and both protocols (one-shot and five-shot). In some instances, the differences were statistically significant, as indicated by the STDs.

To conclude, the findings suggest that human-defined masks are more effective than random

Table 4. The impact of different similarity benchmarks on TPFSL's performance.

distance	**COVCT**		**SARSCOV2**		**SIRM**	
	1-shot	5-shot	1-shot	5-shot	1-shot	5-shot
Mahalanobis	67.5±1.1	84.3±0.7	77.4±1.1	91.2±0.7	70.3±0.8	68.4±0.5
Cosine	67.1±1.0	84.2±0.7	76.6+1.1	91.5±0.7	70.9±0.8	88.1±0.5
Manhattan	68.2±1.0	86.1±0.8	79.6±1.0	92.6±0.7	71.4±0.8	90.2±0.5
Euclidean	**69.3±1.0**	**86.2±0.6**	**80.5±1.0**	**92.8±0.6**	**72.6±0.8**	**90.3±0.4**

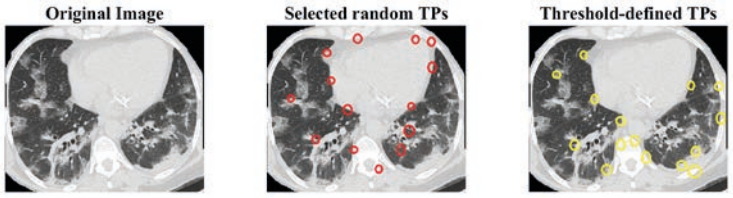

a) COVI-19

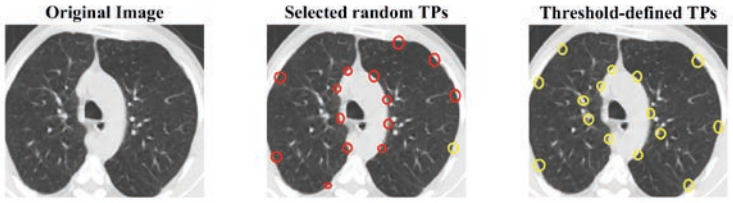

b) Non-COVID-19

Figure 9. Typical examples of extracted TPsfor six different images from all datasets.

Table 6. The performance comparison between Selected random masks and human-defined (Threshold)

Method	**COVCT**		**SARSCOV2**		**SIRM**	
	1-shot	5-shot	1-shot	5-shot	1-shot	5-shot
Randomly generated masks	78.3±1.1	90.9±0.6	71.2±1.0	90.1±0.5	69.3±1.2	87.4±0.9
human-defined (Threshold)	**80.5±1.0**	**92.8±0.6**	**72.6±0.8**	**90.9±0.4**	**69.9±1.1**	**89.6±0.8**

masks in the mask selection task. However, the choice of method may vary depending on several factors, such as the specific task requirements and available resources. Nonetheless, it is important to note that the study had limitations as it only examined two protocols (one-shot and five-shot), and the generalizability of the results to other protocols remains uncertain. Additionally, the study did not explore the potential impact of various elements, such as the size and complexity of the masks or the expertise of the human annotators, on the performance of the different methods.

Further research is required to investigate these factors and extend the results to other tasks and protocols. Such studies would provide deeper insights into the performance of different methods and facilitate informed decisions regarding their selection in practical applications.

This section presents a comprehensive evaluation of TPFSL, a proposed model, on three datasets, namely SARSCOV2, COVCT, and SIRM, and compares its performance to benchmark models. As shown in Table 2, TPFSL outperformed all benchmark models by a significant margin, achieving an average improvement of 4.50% and 4.43% in one-shot and five-shot classification tasks, respectively. In addition, TPFSL outperformed the state-of-the-art model, ProtoNet, by 12.966% and 11.033% in one-shot and five-shot classification tasks, respectively, across all three datasets.

To assess the impact of using a deeper Conv-6 backbone, TPFSL's performance was evaluated, and the results demonstrated that TPFSL's significant improvements were retained. Table 3 compared TPFSL's performance to that of an ensemble of prototypical networks, and TPFSL's performance was evaluated with shared weights across all TPs. The results showed that TPFSL significantly outperformed the ensemble of ProtoNets, even with shared weights across TPs. Furthermore, the performance of TPFSL was minimally affected when using shared weights across TPs.

To investigate how the number of TPs affects TPFSL's performance on the three datasets, a study was conducted and presented in Figure 6. The findings showed that increasing the number of TPs consistently enhanced TPFSL's performance on all datasets. Surprisingly, even including a single TP, which corresponds to a 10 dB threshold of the whole image TP, led to an 11% and 6% improvement in ProtoNet's effectiveness on COVCT in one-shot and five-shot classification tasks, respectively. On the SARSCOV2, TPFSL achieved superior performance compared to all benchmarks with only 8 TPs and outperformed ProtoNet by 8% and 18% in one-shot and five-shot classification tasks, respectively.

In conclusion, TPFSL demonstrated excellent performance over state-of-the-art models on three diverse datasets, suggesting that it is a promising model for few-shot image classification tasks and is robust to variations in the number of TPs and backbone architecture.

4.7 Time complexity analysis

Calculating the order of time complexity in Big O notation for the TPFSL technique involves thorough knowledge of the algorithm's internal operations, such as the structure of its computations, the structure of its data processing, and the effectiveness of its learning mechanism. The following is a high-level description of the methodology used to determine TPFSL's temporal complexity:

Data Processing: First, assume that the time required to process each data point (or image) is O(d), where d is the dimension of the data point or its complexity. Processing the complete dataset will take O(Nd) time if there are N data points in total.

Model Architecture: The complexity introduced by the model's architecture is O(Lm) if there are L layers in the model and if each layer requires O(m) operations per data point.

Learning Mechanism: Third, an adaptive learning mechanism is commonly used in FSL to process new information swiftly. The complexity of the learning mechanism would be O(kp) if the adaptation required iterating over k shots, with each iteration requiring O(p) operations.

Overall Time Complexity: Taking all of this into account, we get an overall time complexity for the TPFSL method of O($Nd + Lm + kp$). This approach, however, is oversimplified since it presumes that the processes in question are independent and occur in a predetermined order.

Practical Considerations: Although the theoretical time complexity may be fixed, the actual runtime may vary greatly depending on practical considerations such as parallel processing, algorithm improvements, and the efficiency of the underlying hardware.

It should be highlighted that for real-time applications, the inference time is more significant than the training time. Offline training of a TPFSL model with a small sample size enables rapid deployment for real-time inference.

5 Conclusion

In this study, the authors developed the TPFSL method as an innovative strategy for the early identification and diagnosis of COVID-19. This method utilizes automated evaluation of paralinguistic elements present in speech signals. One notable benefit of TPFSL is its capacity to improve the ability to generalize models by the utilization of human-interpretable TP dimensions. This technique allows for the amalgamation of outputs from independent TP learners. The evaluation of TPFSL's performance was conducted on three well-established datasets, comparing it to seven benchmark models. The results indicated that TPFSL exhibited superior performance compared to the leading benchmark models in both the one-shot and five-shot classification tasks, with average improvements of 4.50% and 4.43%, respectively. In all datasets examined, the TPFSL method demonstrated a statistically significant enhancement of 12.966% and 11.033%, respectively, as compared to the ProtoNet benchmark in the context of one-shot and five-shot classification tasks. The technique that has been developed exhibits the potential for enhancing the precision and efficiency of COVID-19 diagnosis within clinical environments. In conclusion, the results indicate that TPFSL exhibits potential as a viable method for improving the precision of diagnoses pertaining to these particular illnesses.

However, TPFSL has some limitations that need to be addressed. One major limitation is its heavy reliance on the availability of paralinguistic features in speech signals, which may not always be present in real-world scenarios. Additionally, the evaluation of TPFSL was limited to only three datasets, which may not provide a comprehensive assessment of the model's effectiveness in all scenarios.

In order to augment the capabilities and broaden the scope of the TPFSL model in the field of medical diagnosis, subsequent research should pursue various critical avenues. It is imperative to enhance the generalizability of TPFSL to encompass larger and more diverse datasets. This encompasses not only the expansion of the range of medical data but also the utilization of the model in other categories of biomedical information, including genomic data, imaging modalities, and electronic health records.

Enhancing the interpretability of the acquired representations in TPFSL constitutes another crucial domain. Enhancing the comprehension of the model's diagnostic prediction process will facilitate medical practitioners in making more informed judgments. This may entail the advancement of novel methodologies for displaying and assessing the decision-making processes of the model, particularly in intricate clinical circumstances.

The incorporation of TPFSL with sophisticated machine learning methodologies such as deep learning or transfer learning offers substantial potential. The integration of many components has the potential to improve the diagnostic accuracy and efficiency of the model, particularly in the context of uncommon diseases or complex clinical conditions where access to extensive data is limited.

Furthermore, the exploration of the utilization of TPFSL in the field of customized medicine would represent a highly worthwhile avenue of research. The utilization of Tailored Patient-Focused Strategies for Medical Diagnosis and Treatment has the potential to enhance the efficacy and precision of healthcare interventions by customizing them to specific patient characteristics.

Another intriguing path to be explored is the utilization of TPFSL in real-time diagnostic applications. This entails examining the optimal implementation of the model within clinical contexts to promptly assess patients, with potential advantages in emergency medicine or intensive care settings.

Moreover, the utilization of Temporal Pattern Mining for Sequential Data in the field of predictive health analytics is a promising avenue for further investigation. This encompasses the utilization of the model for the purpose of forecasting the

advancement of diseases, determining patient outcomes, or assessing the probability of disease recurrence. Such applications can play a crucial role in the proactive management of healthcare.

Finally, it is of utmost importance to take into account the ethical ramifications and data privacy issues associated with the utilization of AI models such as TPFSL in the field of medical diagnostics. Subsequent investigations must focus on these dimensions, guaranteeing that the model conforms to ethical norms and legal obligations, all the while upholding patient confidentiality and safeguarding data security.

The proposed research directions seek to make substantial progress in the field of medical diagnostics by utilizing the TPFSL model. This approach is intended to address existing obstacles and predict future requirements in the healthcare sector.

Declaration

Funding

This work was supported by Postdoctoral Program in Jilin Province Postdoctoral Project (Research and Application of Gastrointestinal Tumor Segmentation Methods Based on Deep Learning and Multimodal Images).

Conflicts of interest/ Competing interests

The authors declare that there is no conflict of interest

Code availability

The source code of the models can be available by reasonable request.

References

[1] W.M. Shaban, A.H. Rabie, A.I. Saleh, M.A. Abo-Elsoud, A new COVID-19 Patients Detection Strategy (CPDS) based on hybrid feature selection and enhanced KNN classifier, Knowledge-Based Syst. 205 (2020) 106270.

[2] J. Li, C. Huang, Y. Yang, J. Liu, X. Lin, J. Pan, How nursing students' risk perception affected their professional commitment during the COVID-19 pandemic: the mediating effects of negative emotions and moderating effects of psychological capital, Humanit. Soc. Sci. Commun. 10 (2023) 1–9.

[3] M.M. Islam, F. Karray, R. Alhajj, J. Zeng, A review on deep learning techniques for the diagnosis of novel coronavirus (COVID-19), Ieee Access. 9 (2021) 30551–30572.

[4] Q. Zhang, Y. Wang, R.-T. Bai, B.-R. Lian, Y. Zhang, L.-M. Cao, X-linked Charcot-Marie-Tooth disease after SARS-CoV-2 vaccination mimicked stroke-like episodes: A case report, World J. Clin. Cases. 11 (2023) 464.

[5] T. Sharma, R. Nair, S. Gomathi, Breast cancer image classification using transfer learning and convolutional neural network, Int. J. Mod. Res. 2 (2022) 8–16.

[6] I. Chatterjee, Artificial intelligence and patentability: review and discussions, Int. J. Mod. Res. 1 (2021) 15–21.

[7] W. Dang, L. Xiang, S. Liu, B. Yang, M. Liu, Z. Yin, L. Yin, W. Zheng, A Feature Matching Method based on the Convolutional Neural Network., J. Imaging Sci. Technol. 67 (2023).

[8] P.K. Vaishnav, S. Sharma, P. Sharma, Analytical review analysis for screening COVID-19 disease, Int. J. Mod. Res. 1 (2021) 22–29.

[9] W. Wang, F. Qi, D. Wipf, C. Cai, T. Yu, Y. Li, Z. Yu, W. Wu, Sparse Bayesian Learning for End-to-End EEG Decoding, IEEE Trans. Pattern Anal. Mach. Intell. (2023).

[10] B. Cheng, D. Zhu, S. Zhao, J. Chen, Situation-aware IoT service coordination using the event-driven SOA paradigm, IEEE Trans. Netw. Serv. Manag. 13 (2016) 349–361.

[11] X. Shen, S.-C. Du, Y.-N. Sun, P.Z.H. Sun, R. Law, E.Q. Wu, Advance Scheduling for Chronic care under online or Offline revisit uncertainty, IEEE Trans. Autom. Sci. Eng. (2023).

[12] S. Lu, J. Yang, B. Yang, Z. Yin, M. Liu, L. Yin, W. Zheng, Analysis and Design of Surgical Instrument Localization Algorithm., C. Model. Eng. Sci. 137 (2023).

[13] X. Yi, X. Guan, C. Chen, Y. Zhang, Z. Zhang, M. Li, P. Liu, A. Yu, X. Long, L. Liu, Adrenal incidentaloma: machine learning-based quantitative texture analysis of unenhanced CT can effectively differentiate sPHEO from lipid-poor adrenal adenoma, J. Cancer. 9 (2018) 3577.

[14] Z.A.A. Alyasseri, M.A. Al-Betar, I.A. Doush, M.A. Awadallah, A.K. Abasi, S.N. Makhadmeh, O.A. Alomari, K.H. Abdulkareem, A. Adam, R. Damasevicius, Review on COVID-19 diagnosis models based on machine learning and deep learning approaches, Expert Syst. 39 (2022) e12759.

[15] S. Lawrence, C.L. Giles, Overfitting and neural networks: conjugate gradient and backpropagation, in: Proc. IEEE-INNS-ENNS Int. Jt. Conf. Neural Networks. IJCNN 2000. Neural Comput. New Challenges Perspect. New Millenn., IEEE, 2000: pp. 114–119.

[16] N. Wang, J. Chen, W. Chen, Z. Shi, H. Yang, P. Liu, X. Wei, X. Dong, C. Wang, L. Mao, The effectiveness of case management for cancer patients: an umbrella review, BMC Health Serv. Res. 22 (2022) 1–20.

[17] S.K. Shukla, V.K. Gupta, K. Joshi, A. Gupta, M.K. Singh, Self-aware execution environment model (SAE2) for the performance improvement of multicore systems, Int. J. Mod. Res. 2 (2022) 17–27.

[18] T. Clarke, P. Ayres, J. Sweller, The impact of sequencing and prior knowledge on learning mathematics through spreadsheet applications, Educ. Technol. Res. Dev. (2005) 15–24.

[19] Y. Wang, Q. Yao, J.T. Kwok, L.M. Ni, Generalizing from a few examples: A survey on few-shot learning, ACM Comput. Surv. 53 (2020) 1–34.

[20] J. Vanschoren, Meta-learning, Autom. Mach. Learn. Methods, Syst. Challenges. (2019) 35–61.

[21] T. Hospedales, A. Antoniou, P. Micaelli, A. Storkey, Meta-learning in neural networks: A survey, IEEE Trans. Pattern Anal. Mach. Intell. 44 (2021) 5149–5169.

[22] J.R. Anderson, Is human cognition adaptive?, Behav. Brain Sci. 14 (1991) 471–485.

[23] J.L. McClelland, M.M. Botvinick, D.C. Noelle, D.C. Plaut, T.T. Rogers, M.S. Seidenberg, L.B. Smith, Letting structure emerge: connectionist and dynamical systems approaches to cognition, Trends Cogn. Sci. 14 (2010) 348–356.

[24] Y. Ma, G. Zhong, W. Liu, Y. Wang, P. Jiang, R. Zhang, ML-CGAN: conditional generative adversarial network with a meta-learner structure for high-quality image generation with few training data, Cognit. Comput. 13 (2021) 418–430.

[25] Y. Zhang, B. Lian, S. Yang, X. Huang, Y. Zhou, L. Cao, Metabotropic glutamate receptor 5-related autoimmune encephalitis with reversible splenial lesion syndrome following SARS-CoV-2 vaccination, Medicine (Baltimore). 102 (2023).

[26] Z. Gao, X. Pan, J. Shao, X. Jiang, Z. Su, K. Jin, J. Ye, Automatic interpretation and clinical evaluation for fundus fluorescein angiography images of diabetic retinopathy patients by deep learning, Br. J. Ophthalmol. (2022).

[27] Y. Liu, Y. Wu, X. Shen, L. Xie, COVID-19 multi-targeted drug repurposing using few-shot learning, Front. Bioinforma. 1 (2021) 693177.

[28] Y. Wang, C. Jiang, Y. Wu, T. Lv, H. Sun, Y. Liu, L. Li, X. Pan, Semantic-Powered Explainable Model-Free Few-Shot Learning Scheme of Diagnosing COVID-19 on Chest X-ray, IEEE J. Biomed. Heal. Informatics. 26 (2022) 5870–5882.

[29] W. Li, Diagnose COVID-19 Based on CT Images Using Transfer Learning, in: 2021 2nd Int. Conf. Artif. Intell. Comput. Eng., IEEE, 2021: pp. 740–744.

[30] X. Chen, L. Yao, T. Zhou, J. Dong, Y. Zhang, Momentum contrastive learning for few-shot COVID-19 diagnosis from chest CT images, Pattern Recognit. 113 (2021) 107826.

[31] Y. Ge, Y. Guo, Y.-C. Yang, M.A. Al-Garadi, A. Sarker, Few-shot learning for medical text: A systematic, (n.d.).

[32] Y. Jiang, H. Chen, H. Ko, D.K. Han, Few-shot learning for ct scan based covid-19 diagnosis, in: ICASSP 2021-2021 IEEE Int. Conf. Acoust. Speech Signal Process., IEEE, 2021: pp. 1045–1049.

[33] R. Abdrakhmanov, M. Altynbekov, A. Abu, A. Shomanov, D. Viderman, M.-H. Lee, Few-shot learning approach for COVID-19 detection from X-ray images, in: 2021 16th Int. Conf. Electron. Comput. Comput., IEEE, 2021: pp. 1–3.

[34] M. Abdel-Basset, V. Chang, H. Hawash, R.K. Chakrabortty, M. Ryan, FSS-2019-nCov: A deep learning architecture for semi-supervised few-shot segmentation of COVID-19 infection, Knowledge-Based Syst. 212 (2021) 106647.

[35] P. Singh, P. Mazumder, Dual class representation learning for few-shot image classification, Knowledge-Based Syst. 238 (2022) 107840.

[36] X. Wang, Y. Yuan, D. Guo, X. Huang, Y. Cui, M. Xia, Z. Wang, C. Bai, S. Chen, SSA-Net: Spatial self-attention network for COVID-19 pneumonia infection segmentation with semi-supervised few-shot learning, Med. Image Anal. 79 (2022) 102459.

[37] M. Shorfuzzaman, M.S. Hossain, MetaCOVID: A Siamese neural network framework with contrastive loss for n-shot diagnosis of COVID-19 patients, Pattern Recognit. 113 (2021) 107700.

[38] R. Abdrakhmanov, D. Viderman, K.-S. Wong, M. Lee, Few-Shot Learning based on Residual Neural Networks for X-ray Image Classification, in: 2022 IEEE Int. Conf. Syst. Man, Cybern., IEEE, 2022: pp. 1817–1821.

[39] X. Yang, X. He, J. Zhao, Y. Zhang, S. Zhang, P. Xie, COVID-CT-dataset: a CT scan dataset about COVID-19, (2020).

[40] C. Interiano, S. Muze, B. Turner, M. Gonzalez, B. Rogers, R. Jerris, E. Weinzierl, M. Elkhalifa, V. Leung-Pineda, Dataset for longitudinal evaluation of the Abbott ARCHITECT SARS-CoV-2 IgM and IgG assays in a pediatric population divided by age, Data Br. 36 (2021) 107110.

[41] E. Neri, V. Miele, F. Coppola, R. Grassi, Use of CT and artificial intelligence in suspected or COVID-19 positive patients: statement of the Italian Society of Medical and Interventional Radiology, Radiol. Med. 125 (2020) 505–508.

[42] Y. Zhuang, N. Jiang, Y. Xu, Progressive distributed and parallel similarity retrieval of large CT image sequences in mobile telemedicine networks, Wirel. Commun. Mob. Comput. 2022 (2022) 1–13.

[43] S. Lu, B. Yang, Y. Xiao, S. Liu, M. Liu, L. Yin, W. Zheng, Iterative reconstruction of low-dose CT based on differential sparse, Biomed. Signal Process. Control. 79 (2023) 104204.

[44] F. Pahde, M. Puscas, T. Klein, M. Nabi, Multimodal prototypical networks for few-shot learning, in: Proc. IEEE/CVF Winter Conf. Appl. Comput. Vis., 2021: pp. 2644–2653.

[45] Y. Gong, Y. Yue, W. Ji, G. Zhou, Cross-domain few-shot learning based on pseudo-Siamese neural network, Sci. Rep. 13 (2023) 1427.

[46] X. Xu, Z. Wang, Z. Chi, H. Yang, W. Du, Complementary features based prototype self-updating for few-shot learning, Expert Syst. Appl. 214 (2023) 119067.

[47] Z. Wang, P. Ma, Z. Chi, D. Li, H. Yang, W. Du, Multi-attention mutual information distributed framework for few-shot learning, Expert Syst. Appl. 202 (2022) 117062.

[48] B. Oreshkin, P. Rodríguez López, A. Lacoste, Tadam: Task dependent adaptive metric for improved few-shot learning, Adv. Neural Inf. Process. Syst. 31 (2018).

[49] P. Tian, W. Li, Y. Gao, Consistent meta-regularization for better meta-knowledge in few-shot learning, IEEE Trans. Neural Networks Learn. Syst. 33 (2021) 7277–7288.

[50] J. Snell, K. Swersky, R. Zemel, Prototypical networks for few-shot learning, Adv. Neural Inf. Process. Syst. 30 (2017).

[51] X. Luo, H. Wu, J. Zhang, L. Gao, J. Xu, J. Song, A Closer Look at Few-shot Classification Again, ArXiv Prepr. ArXiv2301.12246. (2023).

[52] X. Li, M. Khishe, L. Qian, Evolving deep gated recurrent unit using improved marine predator algorithm for profit prediction based on financial accounting information system, Complex Intell. Syst. (2023) 1–17.

[53] L. Qian, J. Bai, Y. Huang, D.Q. Zeebaree, A. Saffari, D.A. Zebari, Breast cancer diagnosis using evolving deep convolutional neural network based on hybrid extreme learning machine technique and improved chimp optimization algorithm, Biomed. Signal Process. Control. 87 (2024) 105492

[54] Y. Zhang, Y. Guo, Y. Jin, Y. Luo, Z. He, H. Lee, Unsupervised discovery of object landmarks as structural representations, in: Proc. IEEE Conf. Comput. Vis. Pattern Recognit., 2018: pp. 2694–2703.

Hui Liu was born in Changchun, Jilin, P.R. China, in 1982. She received the Ph. D. from Jilin University, P.R. China. Now, she works in School of Mathematics and Statistics, Changchun University of Technology. Her research interests include Tumor recognition and diagnosis, tumor pathology, and image data analysis.
https://orcid.org/0009-0007-6877-0094

Chunjie Wang born in AnShan, LiaoNing , P.R. China, in 1979.She is a Professor, Doctoral Supervisor, Dean .She works in the School of Mathematics and Statistics ,Changchun University of Technology. Her research interests include survival analysis .
https://orcid.org/0000-0001-7808-4900

Xin Jiang was born in Changchun, Jilin, P.R. China, in 1986. She received the Ph. D. from Jilin University, P.R. China. Now, she works in College of Basic Medical Sciences, Jilin University. Her research interests include Tumor recognition and diagnosis, tumor pathology, and image data analysis.
https://orcid.org/0000-0003-3814-7414

Mohammad Khishe received a B.Sc. degree in Maritime Electronics and Communication Engineering from Imam Khomeini Maritime Sciences University, Nowshahr, Iran in 2007 and also, M.Sc. and Ph. D. degrees in Electronic Engineering from Islamic Azad University, Qazvin branch, and Iran University of Science and Technology, Tehran in 2012 and 2017, respectively. Currently, he is associate professor at Imam Khomeini Maritime Sciences University, Nowshahr, Iran. His research interests are Optimization, Artificial Neural Networks, Meta-heuristic Algorithms, Sonar and Radar Signal Processing.
https://orcid.org/0000-0002-1024-8822